Inverting magnetotelluric data with distortion correction –
Stability, uniqueness and trade-off with model structure

M. Moorkamp[1], A. Avdeeva[2], Ahmet T. Basokur[3] and Erhan Erdogan[4,5]

[1]*Ludwig-Maximilians-Universität München, Theresienstrasse 41, München,*

[2] *Complete MT Solutions Inc., Manotick, Canada*

[3] *Geophysical Engineering Department, Faculty of Engineering, Ankara University, Gölbasi, Ankara, Turkey*

[4] *Enerjeo Kemaliye Enerji Üretim A.Ş., Kavacik Meydani, Energy Plaza Kat: 8, 34805, Beykoz, Istanbul, Turkey*

[5] *now at: Phoenix Geophysics Limited, Toronto, Ontario, Canada*

SUMMARY

Static distortion of magnetotelluric data is a common effect that can impede the reliable imaging of subsurface structures. Recently we presented an inversion approach that includes a mathematical description of the effect of static distortion as inversion parameters and demonstrated its efficiency with real data. We now systematically investigate the stability of this inversion approach with respect to different inversion strategies, starting models and model parametrizations. We utilize a dataset of 310 magnetotelluric sites that has been acquired for geothermal exploration. In addition, to impedance tensor estimates over a broad frequency range, the dataset also comprises transient electromagnetic measurements to determine near surface conductivity and estimates of distortion at each site. We therefore can compare our inversion approach to these distortion estimates and the resulting inversion models. Our experiments show that inversion with distortion correction produces stable results for various different inversion strategies and for different starting models. Compared to inversion without distortion correction, we can reproduce the observed data better and reduce subsurface artefacts. In contrast, shifting the impedance

curves at high frequencies to match the transient electromagnetic measurements reduces the misfit of the starting model, but does not have a strong impact on the final results. Thus our results suggest that including a description of distortion in the inversion is more efficient and should become a standard approach for magnetotelluric inversion.

1   INTRODUCTION

In recent years three-dimensional inversion of magnetotelluric (MT) data has established itself as a routine method to image the subsurface (e.g. Miensopust 2017). The free availability of three-dimensional MT inversion algorithms such as ModEM (Kelbert et al. 2012) and WSINV3D (Siripunvaraporn 2012) has made such approaches feasible for practitioners and has resulted in a number of studies demonstrating the potential benefits of magnetotelluric imaging on different scales ranging from near-surface waste-site investigations (e.g. Newman et al. 2003) to natural resource exploration (e.g. Hübert et al. 2012) and imaging of the structure of the lithosphere (e.g. Meqbel et al. 2014).

While these successful studies showcase how magnetotellurics can be used to improve our understanding of the Earth, several challenges remain. From a computational point of view, the existing inversion codes still require compromises between sufficiently fine discretization, large model grids that cover all areas of interest for extensive surveys and the time and memory it takes to perform the computations. However, increasing memory, computational power and parallel computing approaches make this a temporary rather than a fundamental problem. With increasing interest in marine studies, the role of bathymetry and the impact on the inversion results becomes more and more important. Here, finite-element calculations on unstructured meshes (e.g. Grayver 2015) promise better discretization of the bathymetry in critical areas and thus precise modeling results.

Despite these tremendous advances, it will not be possible to completely capture the heterogeneity of the subsurface on all scales for the foreseeable future. This poses a problem for magnetotelluric imaging, as small structures on the order of centimeters to meters can influence magnetotelluric impedances at all frequencies (Jiracek 1990; Chave & Jones 2012). This phenomenon is known as static distortion and can occur in any environment. If not handled properly, static distortion can cause severe artifacts in any inversion of magnetotelluric data (Miensopust et al. 2013; Avdeeva et al. 2015).

Given the ubiquity of static distortion, a variety of approaches has been developed to identify distortion and remove as much as possible of it from the observed impedances. Chave & Jones (2012) describe the theory of static distortion and Bibby et al. (2005) give an overview of the different scenarios in which some of the effects of distortion can be removed. In a general environment where conductivity varies significantly in all spatial directions, three approaches have been previously sug-

gested: i) Pellerin & Hohmann (1990) and Árnason et al. (2010) propose to combine magnetotelluric surveys with transient electrogmagnetic measurements (TEM). TEM can determine the near-surface resistivity without any influence of distortion and thus the high-frequency undistorted magnetotelluric apparent resistivity should match the observed TEM resistivity. This fact can be used to determine a static shift factor for the two off-diagonal elements of the MT impedance. It does not take into account though that static distortion can result in a mixing of undistorted impedance elements and thus can only partially remedy the effect of distortion. ii) The phase tensor (Caldwell et al. 2004) is a quantity that can be calculated from observed magnetotelluric impedances and is not affected by static distortion. First results using the phase tensor for inversion are encouraging (Patro et al. 2012). The transformation from impedance to phase tensor reduces the number of independent observables from eight for the MT tensor to four for the phase tensor though and suggests a potential loss of information and consequently resolution. However, there are currently no systematic studies investigating this effect. ii) Alternatively, some studies have used a thin surface layer in their inversion models that is excluded from regularization and intended to mimic the effect of static distortion on the data (Kelbert et al. 2012; Meqbel et al. 2014). Even though the resulting structures in the model are typically larger than the causative bodies for the distortion, this approach appears to be able to account for significant parts of the distortion effect. Having large variations in conductivity in the shallow parts of the model can affect the numerical stability of the forward calculation and in some cases these structures have an effect on the deeper parts of the model.

We recently presented an alternative approach to compensating for static distortion (Avdeeva et al. 2015) which has already been adopted in practice (Wannamaker 2016; Gribenko & Zhdanov 2017; Soyer et al. 2018; Moorkamp et al. 2019). Instead of reducing the number of observables or introducing artificial structures in the inversion models, we include the distortion matrix for each site as parameters in the inversion. First tests on a synthetic benchmark model (Miensopust et al. 2013; Avdeeva et al. 2015) show the success of this method. Even in the presence of significant distortion, we can reconstruct the conductivity of the subsurface with a resolution that is comparable with the inversion of undistorted data.

We now systematically examine the practical implications of using this approach with field data. In particular, we will focus on comparing the effect of different inversion strategies and assessing the stability of the results. We use a dataset acquired in the Gediz Graben, western Turkey, for geothermal prospecting to examine the improvements that can be gained from correcting for distortion within the inversion and to develop recipes that can be used for other surveys. This dataset has a number of properties that make it particularly suitable for such an investigation: i) The data is high quality and acquired on a dense array of sites. ii) There are clear signs of distortion at a number of sites. iii)

Transient electromagnetic data (TEM) have been acquired at each MT site to determine a distortion free estimate of 1D near surface resistivity. iv) A number of boreholes have been drilled in the area that can be used to verify some of the structures in the inversion models.

The existence of TEM data gives us a quantity to use for comparison with the distortion retrieved by our approach and provides us with a benchmark beyond the comparison of different models from different approaches. Also, we can see in how far the 1D approximation used in the TEM correction approach is valid. In the following we will briefly describe the main ideas behind the distortion correction algorithm. We will then compare a number of different 3D MT inversion approaches for the field dataset, and investigate to which extent the different inversions can explain different aspects of the data. We will also compare the resulting models with borehole data from the area to see to which degree the major structures in our models match with boundaries in the boreholes. Finally, we will look at the recovered distortion at different sites and the statistical distribution of the values. As the focus of this paper is on the inversion approach, we will not provide a full interpretation of the results in terms of the geothermal prospectivity, but give a brief assessment of the value of the results in the context of geothermal exploration.The general geology and electrical resistivity structure of the Gediz Graben are discussed in Erdoğan & Candansayar (2017). Hacıoğlu et al. (in press) examine the relation between reservoir types and 3D model derived from MT data in view of fluid transport and clay alteration for another prospect in the area.

2   MAGNETOTELLURIC INVERSION WITH DISTORTION CORRECTION

A magnetotelluric sounding consists of the horizontal components of the electrical field $\mathbf{E}$ and the magnetic field $\mathbf{H}$ typically measured in north-south and east-west directions. Using modern processing algorithms (e.g. Chave & Thomson 2004), we can estimate the frequency dependent, complex magnetotelluric impedance tensor $\mathbf{Z}$, viz.

$$\left(\begin{array}{c} E_x \\ E_y \end{array} \right) = \left(\begin{array}{cc} Z_{xx} & Z_{xy} \\ Z_{yx} & Z_{yy} \end{array} \right) \left(\begin{array}{c} H_x \\ H_y \end{array} \right). \tag{1}$$

The magnetotelluric impedance and and estimation of the error of its elements provides the input to MT inversion algorithms to recover the conductivity structure of the Earth. The frequency dependence of the impedance tensor provides depth resolution with lower frequencies penetrating deeper into the Earth and consequently sensing structures at greater depth. Typical depths of investigations can range from tens of meters in the kilohertz range to several hundred kilometers at periods of several hours.

One problem that regularly occurs in practice is the phenomenon of static distortion. Here, small structures on the order of meters or less can affect the magnetotelluric impedance at all frequencies

due to charge accumulation at the boundaries (Berdichevskiy & Dmitriev 1976). The effect of the distortion can be described by multiplication of the undistorted impedance tensor with a frequency independent, real matrix $\mathbf{C}$, viz.

$$
\mathbf{Z}^{obs}(\omega) = \mathbf{C}\mathbf{Z}(\omega) = \begin{pmatrix} C_{xx}Z_{xx} + C_{xy}Z_{yx} & C_{xx}Z_{xy} + C_{xy}Z_{yy} \\ C_{yx}Z_{xx} + C_{yy}Z_{yx} & C_{yx}Z_{xy} + C_{yy}Z_{yy} \end{pmatrix}.
\tag{2}
$$

If the effect of distortion is not considered in the inversion of the observed impedance $\mathbf{Z}^{obs}$, it can cause artefacts in the resulting models (Miensopust et al. 2013; Avdeeva et al. 2015). Given that the problem of static distortion has been known for years, a variety of approaches have been developed depending on the dimensionality of the impedance tensor (e.g. Jiracek 1990; Groom & Bahr 1992; Jones 2011). For a general three-dimensional environment current approaches include inverting the distortion free phase-tensor (Caldwell et al. 2004; Patro et al. 2012), determining an approximation of the diagonal elements of the distortion matrix from TEM measurements (Árnason et al. 2010), or allowing for a highly heterogeneous near surface layer in the model in order to mimic the effect of distortion (Kelbert et al. 2012). A more detailed overview of these different approaches can be found in Avdeeva et al. (2015) and Miensopust (2017).

In Avdeeva et al. (2015) we also describe the mathematical details of our inversion approach, so we only summarize the main ideas here. We include the four unknown elements of the distortion matrix $\mathbf{C}$ at each site as additional parameters in the inversion. Thus in addition to the M elements of conductivity σ in each model cell, we have an additional $4 * N$ distortion parameters, where N is the number of sites. Our objective function φ then consists of the data misfit term φ_d and two regularization terms,

$$
\varphi(\boldsymbol{\sigma}, \mathbf{C}, \lambda, \nu) = \varphi_d(\boldsymbol{\sigma}, \mathbf{C}) + \lambda\varphi_s(\boldsymbol{\sigma}) + \nu\psi(\mathbf{C}) \xrightarrow[\boldsymbol{\sigma}, \mathbf{C}]{} \min.
\tag{3}
$$

φ_s is the standard Tikhonov regularization to ensure a smooth model, while ψ regularizes the distortion by penalizing deviations from an identity matrix, i.e. the undistorted case. λ and ν are the Lagrange multipliers for the smoothness and distortion regularization terms, respectively. These are a chosen by the user and fixed throughout an inversion run. We use a limited-memory quasi-Newton approach (Nocedal 2006; Avdeeva & Avdeev 2006) to minimize the objective function. The forward engine for our inversion is the integral-equation base modeling x3d (Avdeev et al. 2002) and we calculate the gradients of the objective function using an adjoint approach (Avdeev & Avdeeva 2009; Avdeeva et al. 2015).
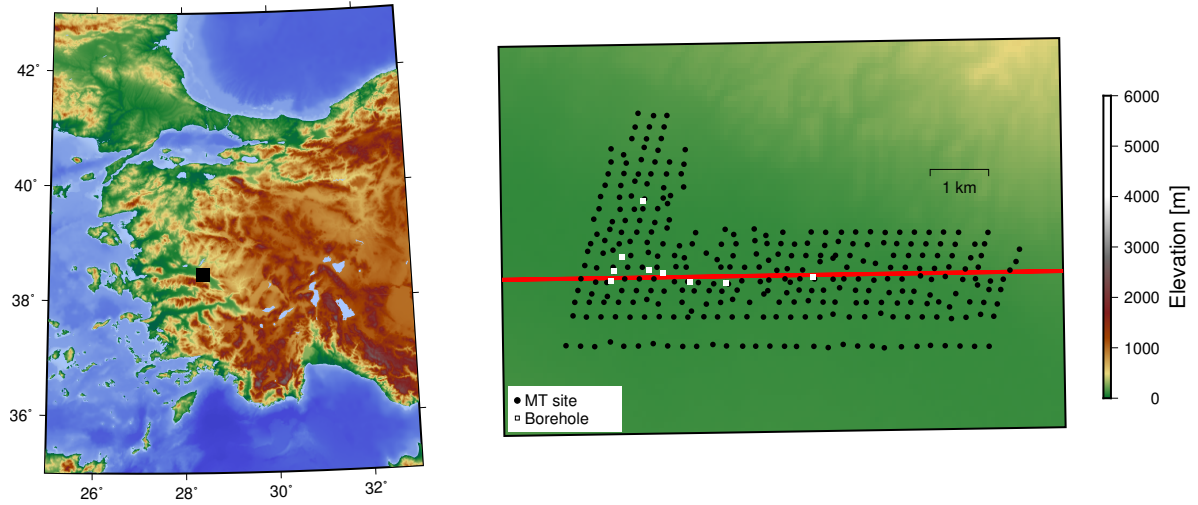
Figure 1. Location of the magnetotelluric survey (left) and overview of the site distribution (right). The black dots show the location of the MT soundings, while the white squares show the location of boreholes in the area. We mark the location of the profile that we use for evaluating the models with a red line. The color indicates elevation.

3   APPLICATION TO A FIELD DATASET

Following the successful application to a synthetic dataset (Avdeeva et al. 2015), we apply our approach to a real field dataset. This 3D array of measurements was acquired in 2013 by Enerjeo to assess the prospectivity of the area for geothermal energy generation. Figure 1 shows the location of the survey in the Gediz Graben in western Turkey and the distribution of MT sites and boreholes in the area.

The geology of the Aegean region is explained by extensional tectonics and metamorphic core complexes. Different concepts exist about the beginning and the mechanism of the extension and these are discussed in Seyitoğlu & Veysel (2015). The Gediz graben is an actively growing asymmetric graben within this extensional setting (Çiftçi & Bozkurt 2010). The graben fillings consist of recent alluvium, continental clastics of claystone, sandstone and gravel that overlie unconformably the metamorphic basement. Coarse grained alluvial deposits dominate the southern margin and grade into ner fractions of uvial and/or lacustrine deposits to the north (Çiftçi & Bozkurt 2009). The core rocks of the metamorphic basement are dominantly gneiss species and the cover rocks are schist and marble that are formed of low grade metamorphic rocks (Seyitoğlu & Veysel 2015). High angle normal faults bounding the graben lead to hot water circulation and outflowing. One possible explanation of the heat source is high heat flow originating from a shallow mantle as a consequences of crustal thinning (Ulugergerli et al. 2007; Hacıoğlu et al. in press).

For exploration in this setting, the most favorable borehole locations are the intersection of normal
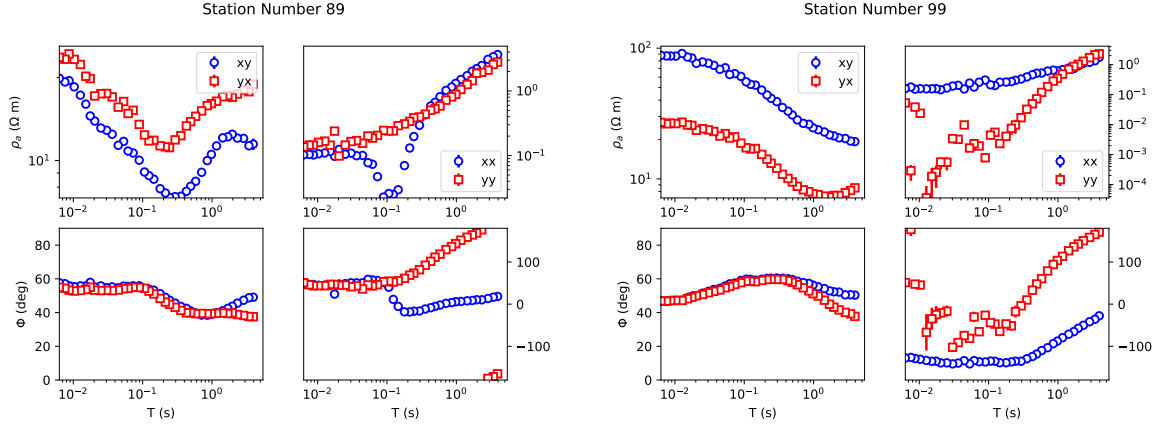
Figure 2. Two data examples showing the generally high data quality. Site 89 (left) shows no or little sign of static distortion, while Site 99 (right) shows clear indication of distortion. At high frequencies the phases of the two off-diagonal elements coincide, while the apparent resistivities differ by a factor of five.

faults and conjugate strike-slip faults since rock deformation leads to an increase in permeability and porosity. Within the Gediz Graben the most productive rock unit is the thick marble lithology that forms a higher-ranking reservoir. In view of the above geological information, the expected resistivity section starts with a thin resistive top layer corresponding to the coarse materials of alluvial fans that overlie a relatively low resistivity layer of claystone and saturated sandstone($< 10\Omega m$). The basement metamorphic rock units have relatively high resistivity values ($> 100\Omega m$). The lowest resistivity values are expected in the fractures and faults filled with conductive fluids, and in the alteration zones consisting of smectite and illite minerals. This geoelectrical setting provides suitable conditions for the application of magnetotellurics for this type of convection dominated-amagmatic geothermal play. The east-west red line in Figure 1 used to evaluate the models is not aligned with the WNW-ESE strike of graben. For this reason, it is expected that the profile intersects firstly the deeper part of the graben and the master normal graben fault. Afterwards the profile extends towards gradually thinning sedimentary cover direction over the footwall side. We will briefly comment on how our models match these expectations in the discussion below.

The survey consists of 310 MT sites with a distance of approximately 300 m between sites. At each site impedance tensors were calculated at frequencies between 10^4 Hz and 0.01 Hz and transient electromagnetic measurements were performed to determine the distortion free near-surface resistivity. Given that the target of the investigation is between 200 m and 3 km depth, for the inversion we focus on the frequency range between 200 Hz and 0.2 Hz. Figure 2 shows the apparent resistivity and phase for the four impedance tensor elements at two exemplary sites.

Both sites demonstrate the high data quality typical for this survey. Both apparent resistivity and phase vary smoothly with frequency for the off-diagonal elements with estimated error bars smaller

than the symbol size. The diagonal elements are also well determined and only for the extremely small values seen at periods between 0.01 s and 0.1 s at site 99, we observe significant scatter due to small electric fields. Site 89 shows little or no sign of static distortion. There is a minor difference in the off-diagonal apparent resistivities at high-frequencies. However, there is also a minor difference in phase, suggesting that this effect could be inductive and not galvanic. In contrast Site 99 shows clear signs of static distortion. At high frequencies the phases of the off-diagonal elements are identical, while the apparent resistivities differ by a factor of 5. This is a clear indication that a small scale structure distorts the electric field in one or both measured directions and it is clear that inverting such data without compensating for the distortion will be problematic. The diagonal elements at both sites are at least a factor of two smaller than the off-diagonal elements and in both cases it is unclear in how far the diagonal elements are affected by distortion.

Together with the MT data, we were provided with estimates of static shift for each site and off-diagonal impedance component, respectively. These estimates were obtained through coincident transient electromagnetic (TEM) measurements at each site and shifting the apparent resistivity curves from MT to match the equivalent resistivities from TEM (Sternberg et al. 1988). Figure 3 shows these estimates converted to an equivalent distortion matrix C. Both the spatial plots and the histograms show, that the diagonal elements of C are not normally distributed, but skewed towards negative values. For most sites the deviation from a unit matrix is relatively small, below -0.2, but some sites reach values up to -0.5. This corresponds to downwards shifts of the apparent resistivity curves of factors 1.4–4. and suggests that on average the resistivity of the near-surface is lower than the apparent resistivity at high frequencies at most sites.

For our inversion experiments we discretize the subsurface into $64 \times 82 \times 32$ rectangular cells. The horizontal dimension of all cells is 200 m×200 m throughout the mesh, while in the vertical direction the cell size increases from 30 m at the surface approximately 600 m at a depth of 6000 m. We use a uniform half-space with a resistivity of 100 Ωm as a starting model. To protect against unrealistically small data errors reported with the measurements, we calculate the Berdichevsky invariant at each frequency and assign the maximum of the reported error and 2% of the invariant as error to all impedance elements at a given frequency and site. Having a uniform error for all four impedance elements diminishes the influence of the smaller elements, e.g. the diagonal elements, however it is the only way to keep the data misfit rotationally invariant. These parameters are identical for all inversion runs that we describe in the following.
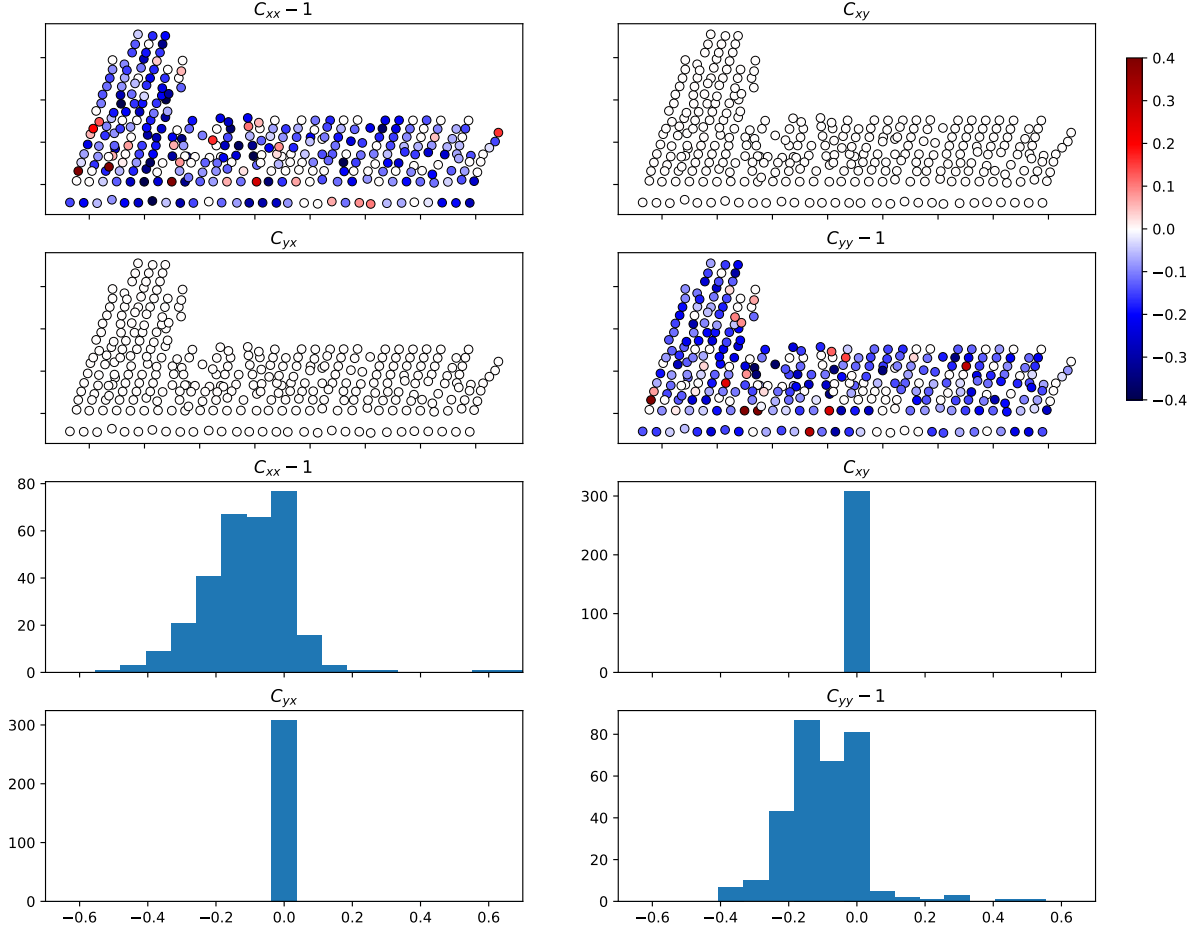
Figure 3. The distortion estimates from coincident TEM measurements. We plot the spatial distribution (top) as well as histograms for all four components of the distortion matrix. Although this method cannot estimate the off-diagonal elements of the distortion matrix, we include the plots for easier comparison with our estimates below. Also, in order to plot all components with the same colour scale, we subtract one from the diagonal elements.

3.1 Inverting with distortion correction

For the first set of experiments we focus on the improved data fit that we can achieve with distortion correction and the difference in the resulting models. We run four different inversions: i) Inverting the magnetotelluric impedances without any correction for distortion within the inversion and ignoring the distortion estimated from the TEM, ii) Correcting for distortion within the inversion, but without considering the TEM measurements, iii) Inverting the magnetotelluric impedances without any correction for distortion, but using the distortion estimates from TEM, iv) Correcting for distortion within the inversion, using the distortion estimates from TEM as a starting point. In all cases we start with a high model regularization value ($\lambda = 5000$) and no distortion correction for the initial iterations, i.e. the first iterations for runs i) and ii) are identical and similarly for runs iii) and iv). This is to ensure that we

have a reasonable average background resistivity before correcting for distortion. We will investigate the importance of this step below.

For all four inversions we follow the same strategy for the regularization. Every 50 iterations, when convergence has slowed, we divide the regularization parameter λ by a factor of ten. For two of the inversion runs, we introduce the distortion correction after the initial 50 iterations. Subsequently, we divide the distortion parameter by the same amount as the model roughness regularization. We performed a large number of inversions with different strategies and this provides a good balance between rapid convergence to small data misfit and significant smoothing to avoid unnecessary scatter in the models.

Figure 4 shows the evolution of the RMS misfit, the model roughness and the magnitude of the distortion as a function of iteration. Although it is not visible at the scale of the plot, the initial RMS when using the TEM correction is slightly lower compared to the data without distortion corrrection. However, after the first few iterations the misfit is practically identical for all four runs until we introduce the distortion correction at iteration 50. We observe that the misfit for the two runs with distortion correction drops and decreases at a faster rate than without distortion correction until we stop the inversion after 200 iterations. At this point both inversions with distortion correction have reached a RMS of 2.0, while the RMS for the inversions without distortion correction is 2.9. At the same time the roughness of the model is a factor of 5 higher for the runs without distortion correction compared to the runs with distortion correction.

While the model roughness and data misfit show similar behaviour regardless of the initial distortion values, the evolution of the distortion is different both in terms of the changes from iteration to iteration and the final value at the end of the inversion. The average deviation from the identity matrix as indicated by the distortion values in Figure 4 is nearly twice as much when we start with the estimates from TEM than when starting from the assumption of no distortion. It is interesting that in both cases though the final estimated distortion is, on average, smaller than the distortion estimates from TEM.

Figure 5 shows a comparison of the distortion values from TEM with the distortion values from the inversion with initial values set from TEM. For each element we plot the two estimates against each other. If the elements were identical, all estimates would plot along the straight line marked in the figure. As we can only estimate the diagonal elements of C from TEM measurements, the diagonal elements are zero and consequently the plots corresponding to those elements show a straight line parallel to the x-axis. For the diagonal elements, we see that most estimates are plotted close to the line indicating equality. The values scatter to both sides of the line demonstrating that for some sites the element estimated from TEM is larger and for other sites the estimate from the inversion is larger. All
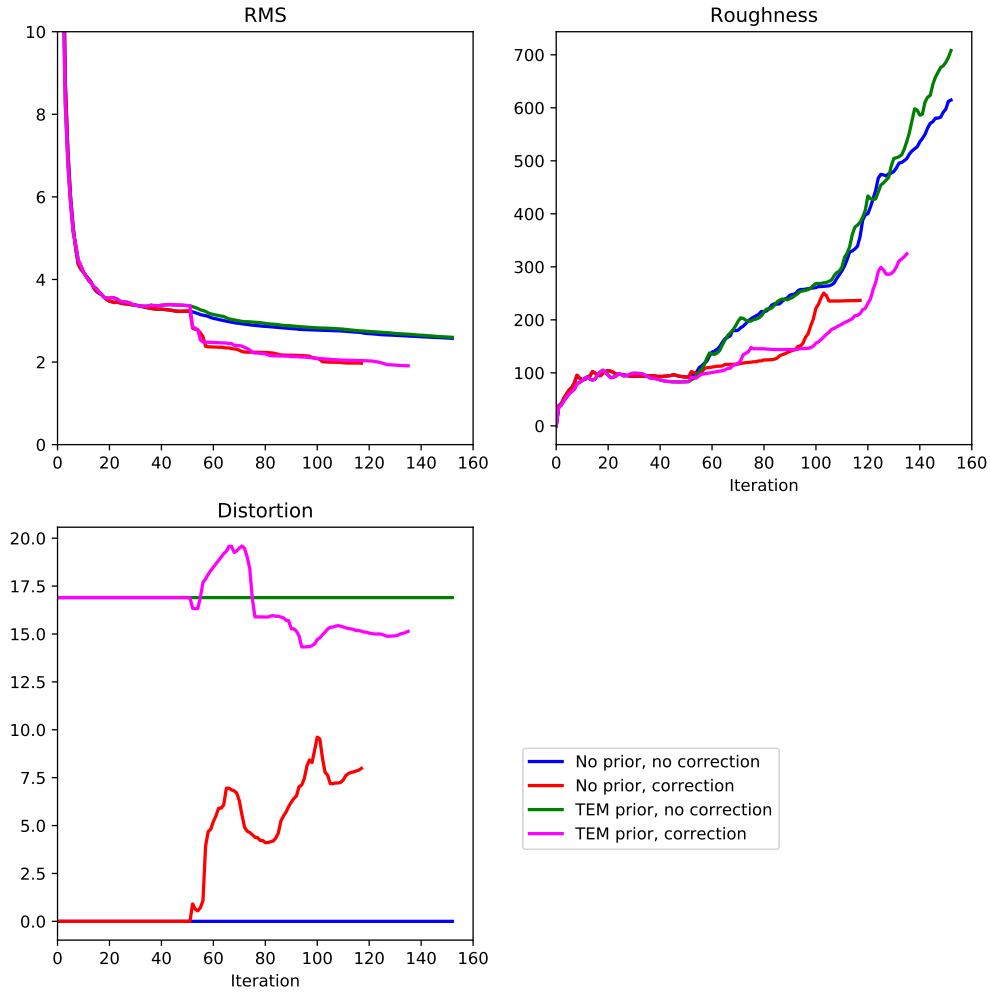
Figure 4. Convergence of the inversion runs for four different scenarios: Without using the prior distortion information from TEM and no distortion correction (blue), without prior distortion and correcting for distortion in the inversion(red), using the prior information from TEM and without distortion correction (green) and using TEM distortion and correcting for distortion (magenta).

in all, it seems that the inversion only made some minor adjustments to the elements of the distortion matrix, mainly to provide estimates for the missing off-diagonal elements.

As discussed above, the distortion estimates provided by the inversion when started without any prescribed values is on average smaller than starting with the TEM estimates. It is therefore interesting to see how the estimates differ between those inversion runs. Figure 6 shows this comparison in the same style as Figure 5. We can see that all four elements scatter around the line with a gradient of
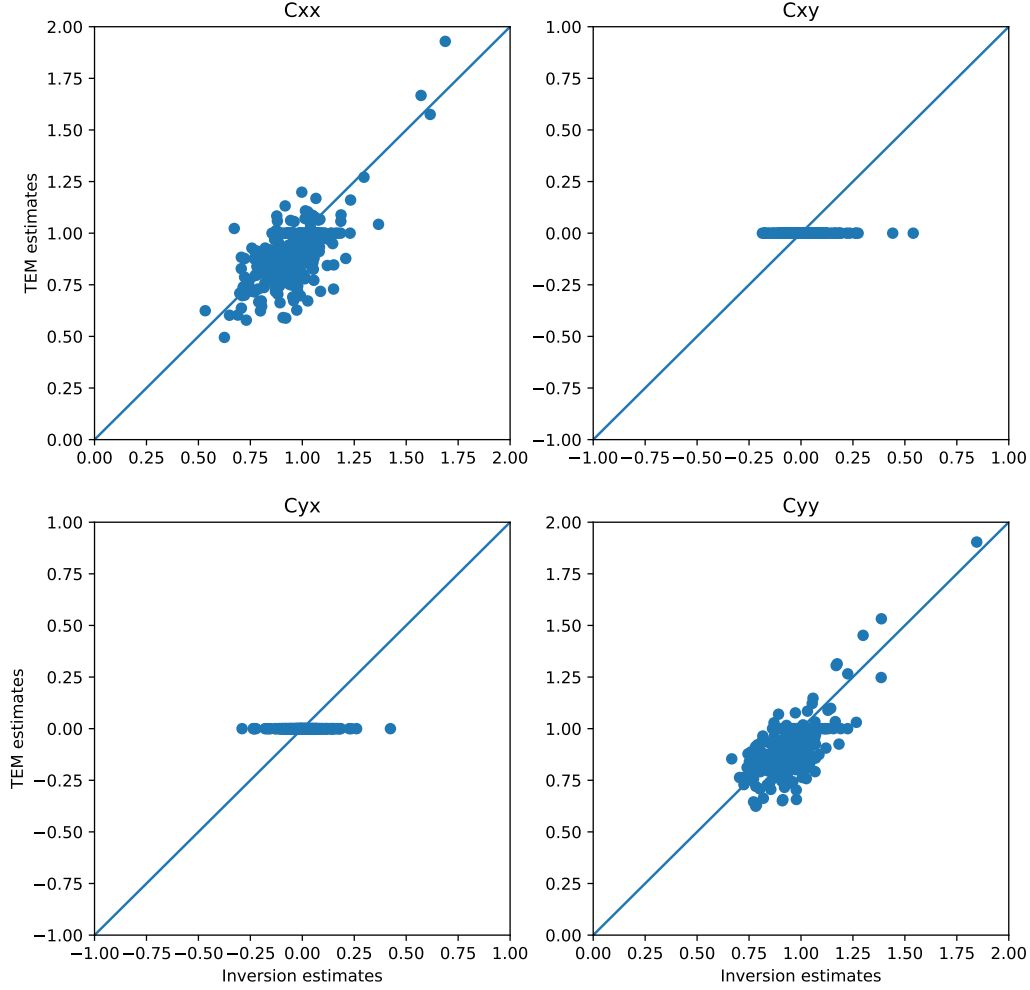
Figure 5. Comparison of the distortion estimates provided by TEM with the distortion estimates retrieved in the inversion. For each element of C we plot the estimates from TEM against the inversion estimates. The line marks the one to one relationship.

unity and the largest/smallest estimates in one inversion run are also the largest/smallest estimates in the other run, so the overall pattern of distortion appears to be robust. Interestingly, the two off-diagonal elements show a very close correspondence between the runs. In comparison, for the diagonal elements many estimates are smaller for the inversion without prior distortion elements as indicated by the reduced range of values. Where the estimates for C_{xx} vary between 0.5-1.75 for the run with prior information from TEM, the range is only 0.75-1.5 for the run without prior information. Furthermore,
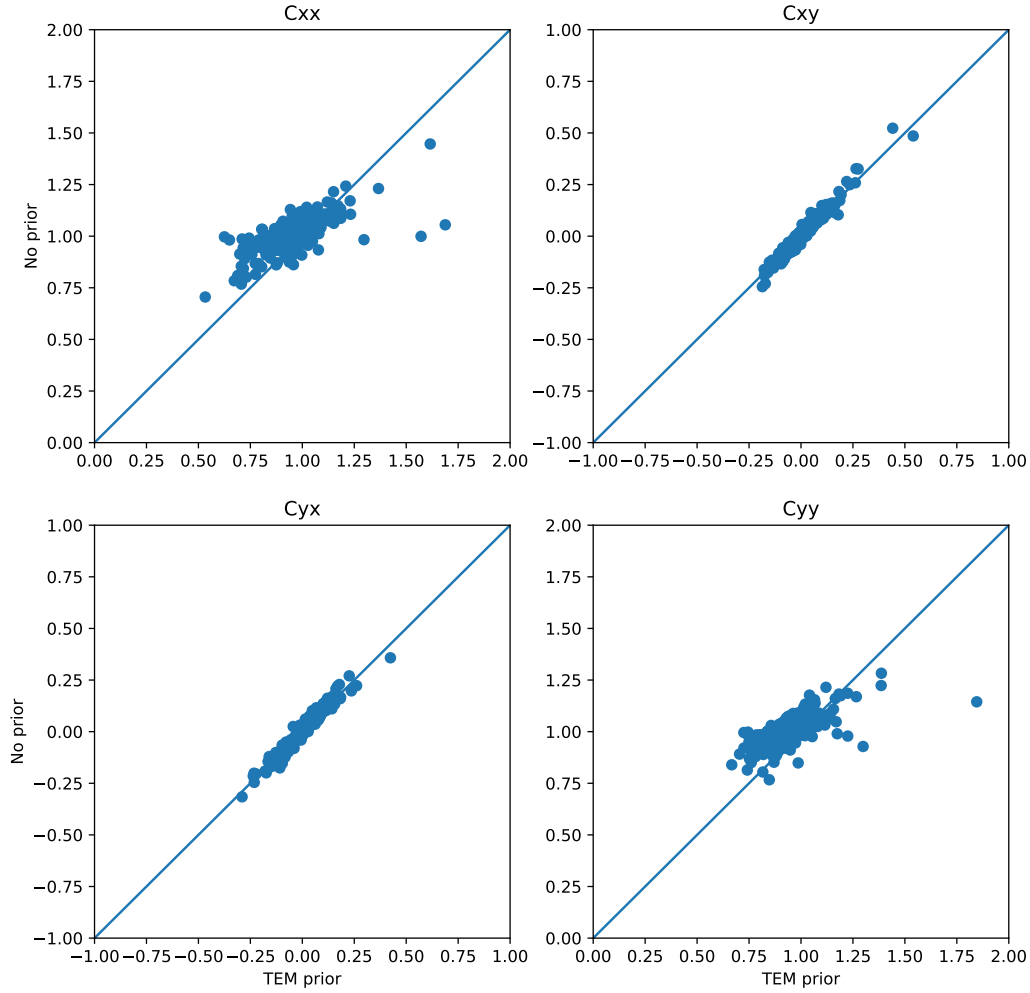
Figure 6. Comparison of the distortion estimates provided by inversion with prior estimates from TEM with the distortion estimates retrieved from inversion where initially we assume no distortion. For each element of C we plot the estimates against each other. The line marks the one to one relationship.

the slope of the points appears to be smaller than unity, confirming that on average the distortion elements are smaller when we start without prior distortion.

Figure 7 shows a comparison of the fit to the observed data at Site 89 for the four different inversion runs. When using the distortion correction in the inversion, we achieve a good fit to all four components of the impedance tensor. This includes the split of apparent resistivity in the off-diagonal components at high frequencies and the behaviour of the phase of the diagonal components. Only at the lowest frequencies of the off-diagonal elements, we observe a split in the phase that is not repro-
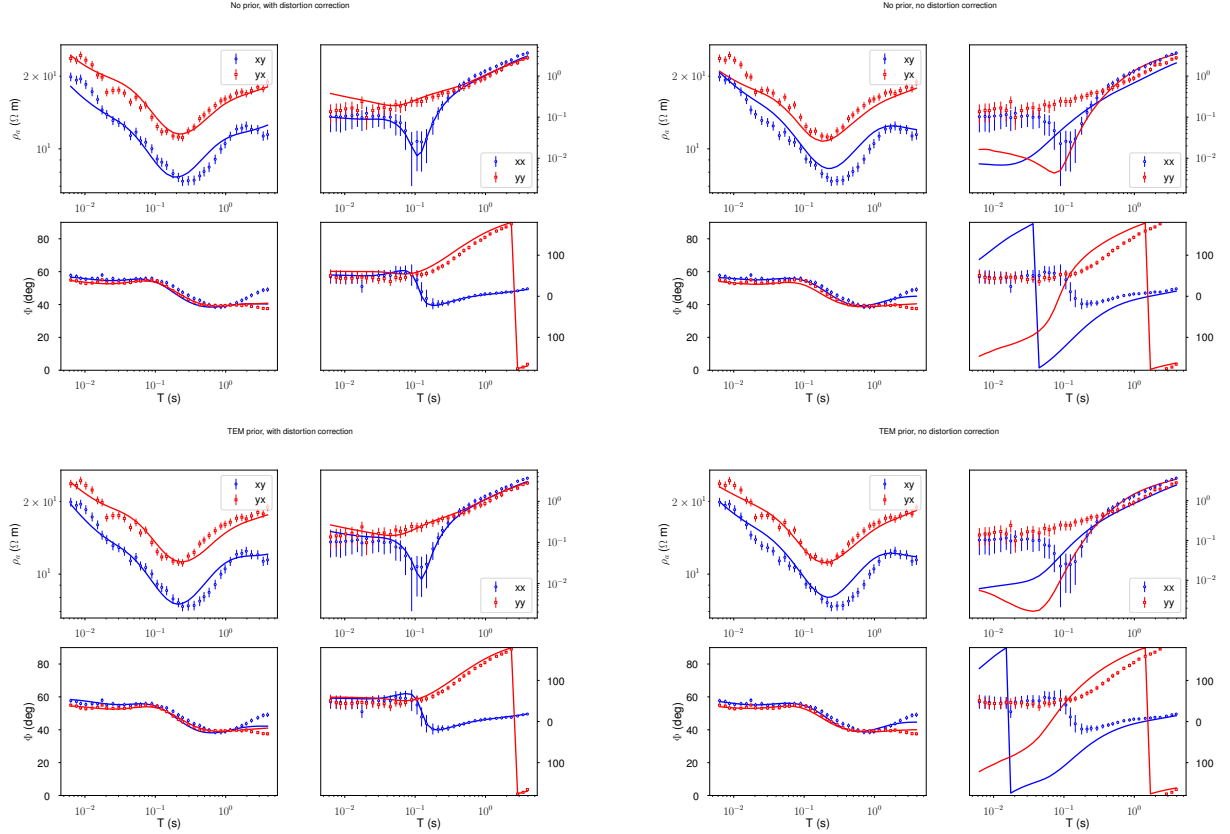
Figure 7. The data misfit for site 89 for the four different inversion runs: starting without any assumed distortion and correcting for distortion in the inversion (top left), starting without distortion and without distortion correction (top right), using the distortion estimates from TEM and correcting for distortion in the inversion (bottom left), using the distortion estimates from TEM without distortion correction (bottom right).

duced by our model. In contrast, the two inversion runs without distortion correction cannot reproduce the general behaviour of the diagonal components of impedance. There is some coincidence of apparent resistivity at low frequencies, but the overall shape of the curves is substantially different for the observed and predicted data for both runs. The off-diagonal components show a similar fit without distortion correction as with distortion correction and, in fact, the lowest frequency data show a somewhat better fit without distortion correction. However, when we do not use the distortion estimates from TEM data, the models cannot reproduce the split of apparent resistivity at high frequencies. It appears that the discretization is too coarse and the regularization too strong to simulate the effect of static shift in this case. However, even if we continue run the inversions with a smaller model roughness regularization, we observe that we introduce even more erratic structures into the model without significant improvement to the data fit.

A comparison of east-west slices through the models from the different inversion runs (Figure 8) illustrates that most of the major features are similar for all inversion runs. We recover a conductive
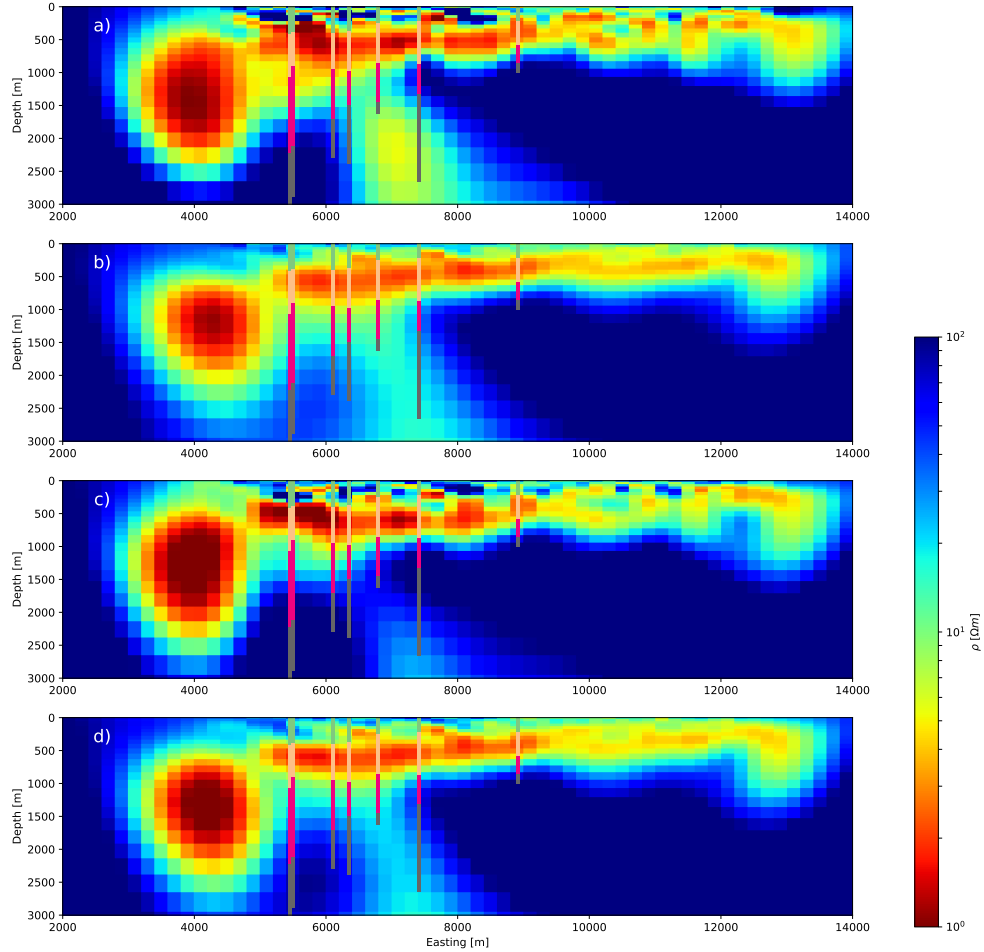
Figure 8. West-east profile through the conductivity model obtained by inverting the observed impedances with different approaches. From top to bottom: Without distortion correction and without considering the TEM data (a), with distortion correction and without considering the TEM data (b), without distortion correction in the inversion, but using the diagonal elements of the distortion matrix obtain from TEM soundings at each site (c), with distortion correction and using the TEM distortion estimates as starting values (d). The coloured bars show the different geological units in the boreholes drilled along this section.

structure at a depth of about 500-1000 m that shows lateral variations in thickness and a displaced conductor towards the western end of the profile. There are, however, significant differences particularly in the shallow part of the model. Both inversions without distortion correction (Figures 8a) and 8c)) exhibit strong variations in conductivity at shallow depths that are not laterally continuous and diffi-
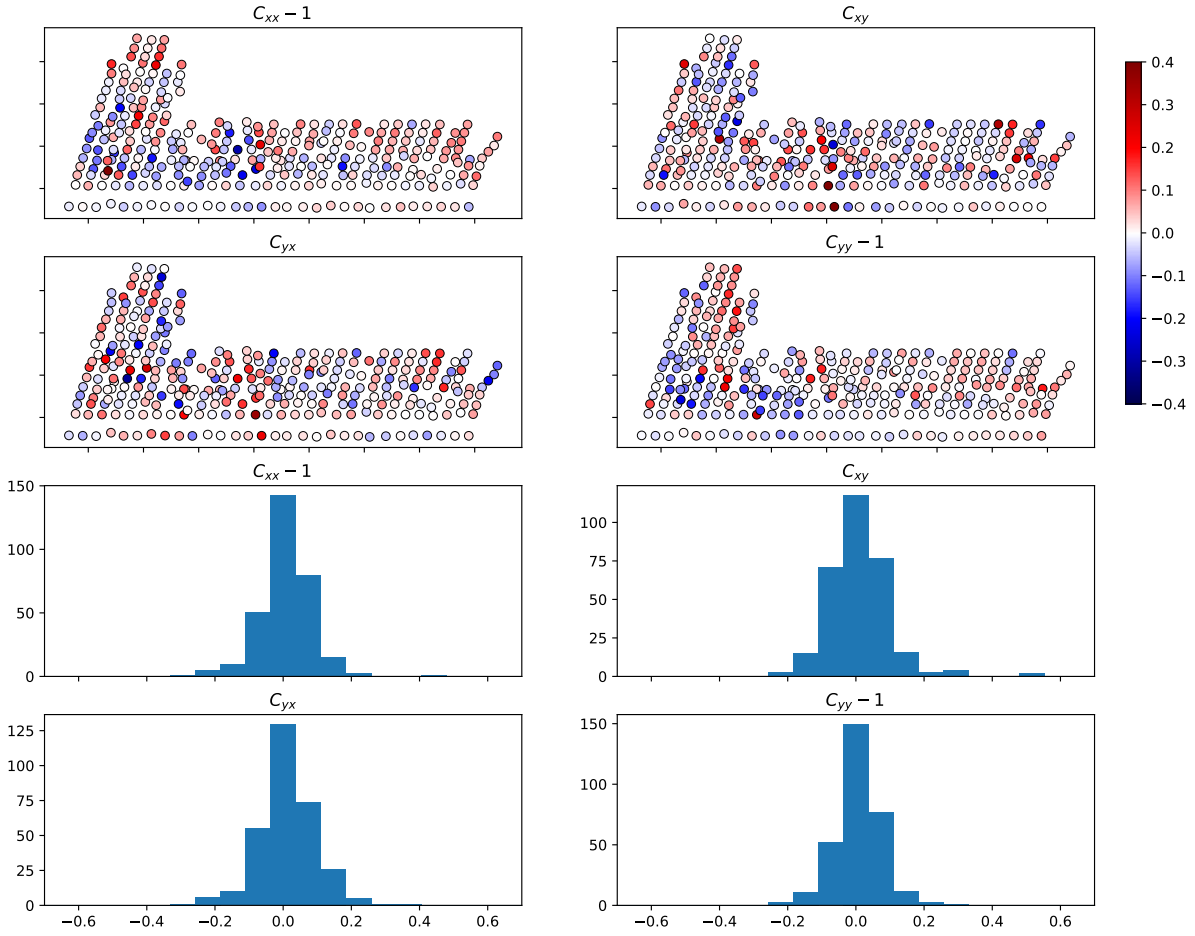
Figure 9. The spatial distribution of the estimated distortion elements (top) and histograms for each element (bottom) for the inversion run with distortion correction and without any prior information.

cult to interpret in terms of geological structure. Towards the eastern end of the profile, these strong variations also affect the main conductor and suggest highly heterogeneous material. In contrast, both inversions with distortion correction result in significantly smoother images. The strong conductivity contrasts at the surface have disappeared and there are only slight lateral variations within the main conductive structure. Also, a comparison with the boundaries of the geological units in the co-located boreholes shows, that the conductivity contrasts agree better with changes in lithology for the two inversions with distortion correction. Overall the results match the expected geological situation described in the introduction. The displacement between the deeper easter conductor and the shallower conductive layer is an expression of normal faulting within the Graben. Furthermore we see the expected thinning of the conductive sediments towards the west. Due to the more coherent resistivity image it can be more easily identified in the results with distortion correction than in the more scattered images without correction.

To round off the discussion in this part, we show the estimated distortion elements for the run

without prior information in Figure 9. In contrast to the prior estimates from TEM (Figure 3), all elements are distributed symmetrically around the identity matrix. To some degree this is a result of the regularization forcing closeness to the identity matrix. However, changing the sign of all elements that plot above zero in the histograms would not change the magnitude of the distortion penalty function. So the inversion algorithm does not favour a symmetric distribution over a skewed one. Looking at the spatial pattern of the elements, we can identify small clusters of mostly positive or negative deviations from the identity matrix. So the recovered distribution is not completely spatially random, but much less coherent than suggested by the TEM estimates. At this point it is unclear how much spatial correlation we can expect and which factors influence the correlation pattern. This would be an interesting avenue for future research.

3.2   Robustness to different settings

The previous experiments have demonstrated that we can obtain models that fit the observed data better and show more spatial coherence when including distortion correction in the inversion. We will now address the question whether the results are robust to different inversion strategies, starting models and choices of spatial discretization. We will first discuss a range of possible strategies and in the next section turn to the influence of the starting model and finally discuss how the choice of model grid influences the results.

From a theoretical perspective it is clear that an inversion with distortion correction but without distortion regularization will be insensitive to the average resistivity of the subsurface. If the elements of the distortion matrix can be freely adjusted, the algorithm can achieve a good fit to the data quickly by adjusting the diagonal elements of $\mathbf{C}$ regardless of the resistivity of the starting model. This phenomenon motivates the strategy in the previous section, where we perform the initial iterations without distortion correction to recover the broad background resistivity and then slowly allow for more distortion in the inversion. We now compare this strategy with inversions where we allow for distortion correction from the first iteration with different penalty values for the distortion regularization. For all experiments we do not use the prior information from the TEM measurements as this information will not be available in most practical applications. As before we concurrently reduce the smoothness and distortion regularization weights by a factor of ten every 50 iterations, only for the inversion with a distortion regularization $\nu = 1$ we keep that value constant throughout the inversion.

The evolution of the different terms of the penalty function with iteration (Figure 10) demonstrates that we achieve a comparable datafit regardless of the inversion strategy. We observed significantly different model roughness and distortion regularization terms though. Interestingly, there is no simple correspondence between the weight for the distortion regularization and the final amount of distortion
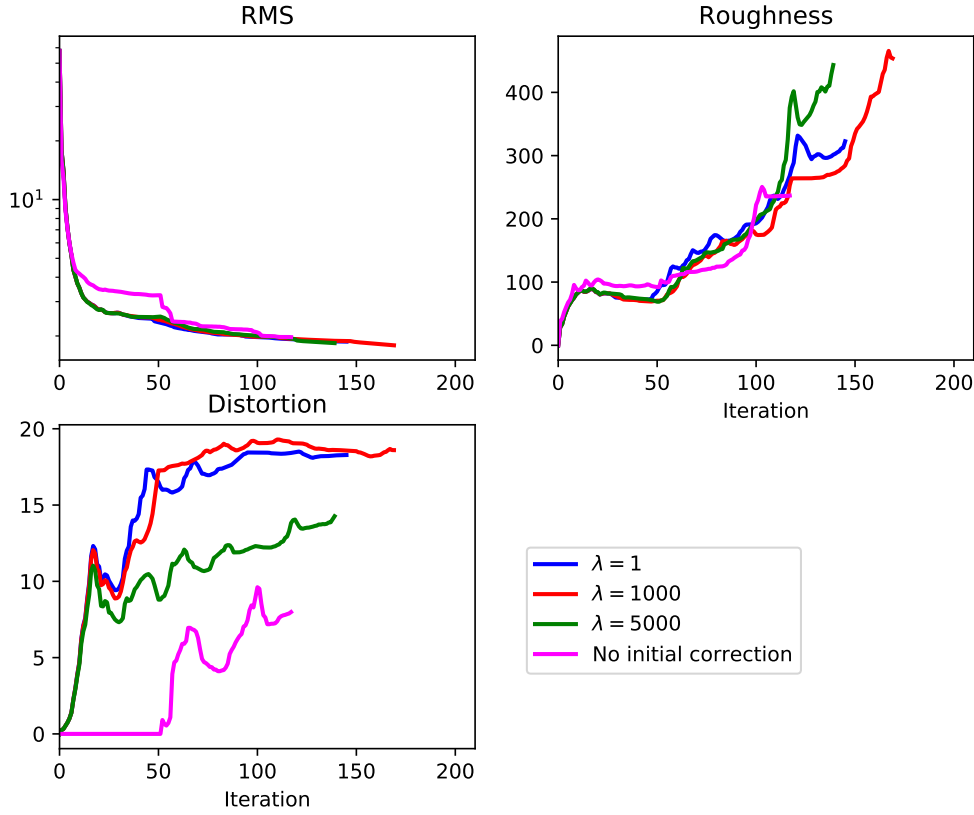
Figure 10. Convergence of the inversion runs for four different scenarios: Allowing for distortion correction in the initial iterations and a small ($\lambda = 1$) weight for the distortion regularization (blue), moderate ($\lambda = 1$, red), high ($\lambda = 5000$, green) values and using the same strategy as described in the previous experiments (magenta). In all cases we did not use any prior distortion information.

in the model, we can see that the distortion for the runs starting with $\nu = 1000$ is marginally higher than for $\nu = 1$. In both cases the overall magnitude of the distortion regularization term of the objective function is small compared to the data misfit term. This changes when we increase the distortion regularization weight to $\nu = 5000$. This results in a significant decrease of the overall distortion. Still, we obtain the smallest distortion regularization values for the previous strategy, where we only allow for distortion after the initial 50 iterations.

Figure 11 shows a comparison of the resulting inversion models. Although we can identify some differences, overall the appearance is very similar and within the range of variations that we would obtain by slightly varying the smoothness regularization in conventional inversion. The strongest difference can be seen in the displaced conductor at the western end of the profile. When we do not initially correct for distortion it is located slightly shallower and extends less deep. All other inver-
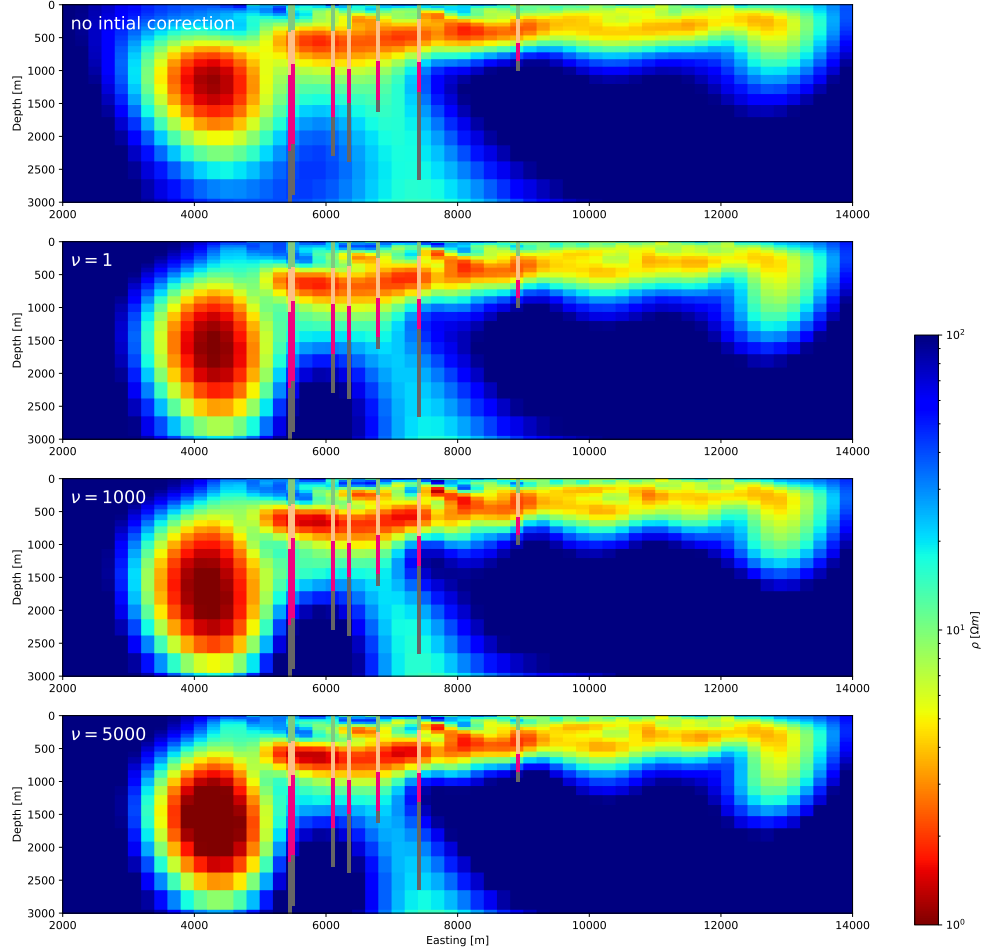
Figure 11. Comparison of the inversion results obtained from different strategies for distortion correction. The value for the distortion regularization is given in each panel and the strategies are described in the text. As in Figure 8 the coloured bars show geological units inferred from boreholes.

sions suggest a marginally larger displacement of this structure compared to the main conductor to the east and reveal more internal heterogeneity within the conductive layer. Given that all models fit the data to the same degree, but the model without initial distortion correction has significantly lower average distortion and model roughness, Occam's Razor suggests that it is the best model. However, we would argue that the differences in the model reflect some of the uncertainty associated with recovering the subsurface structures and all models are reasonable. Depending on other prior knowledge of the region, an interpreter might favour one of these models over the other. Our experiments therefore

indicate that as long as we provide some regularization for the distortion parameters, we can obtain reasonable models and the final results only weakly depend on the chosen distortion regularization value and the strategy employed.

3.3   Robustness to different starting models

Apart from the inversion strategies and parameter setting, the choice of starting model has an impact on the final results in non-linear inverse problems (Tarantola 2004). This is true for conventional MT inversions (Miensopust 2017) and given the discussion of the potential insensitivity to background resistivity could potentially be even more problematic for inversions with distortion correction. All our previous inversions were run with a homogeneous half-space with a resistivity of 100 Ωm. As an alternative we now construct a layered starting model by inverting the Berdichevsky invariant of the average impedance from all sites. This should provide us with an estimate of the average resistivity as a function of depth. Figure 12 shows the resulting layered model. Compared to our chosen half-space, this model is on average more conductive, with resistivities varying around 10 Ωm. We can also identify an expression of the conductor in the previous 3D inversion results as a layer of decreased resistivity at depths between 300-500 m.

For the layered starting model we run the inversion for 50 iterations without distortion correction and then introduce distortion correction as described above. Compared to the homogeneous half-space model the initial RMS drops from 57.8 to 7.0 indicating that this starting model represents the data much better on average. Still, to reach convergence we need a number of iterations comparable to the half-space and the final value for data misfit, model roughness and distortion are comparable to the previous experiment. As before the models from the two inversion runs show very similar features (Figure 13) although the differences are slightly more pronounced than the differences between the four strategies. In particular, we see a more conductive area on the westernmost part of the profile for the layered starting model. This area is not covered by any MT sites and thus we have poor sensitivity in this part of the model. As a consequence, the inversion does not change the resistivities in this region. All other differences are more subtle and as before, the main difference in structure can be seen for the displaced western conductor. Compared to the inversion starting with a half-space, it is thinner and more conductive for the layered starting model. It is well known that magnetotellurics can only resolve the conductance (conductivity-thickness product) of conductive structures well, so this difference is in the null-space of the inversion. Overall, the differences between the models are within the range that would also be expected for conventional inversion without distortion correction.

The recovered distortion estimates (Figure 14) show similar spatial patterns and distribution of the values around the identity matrix. A closer comparison of individual values shows that there are
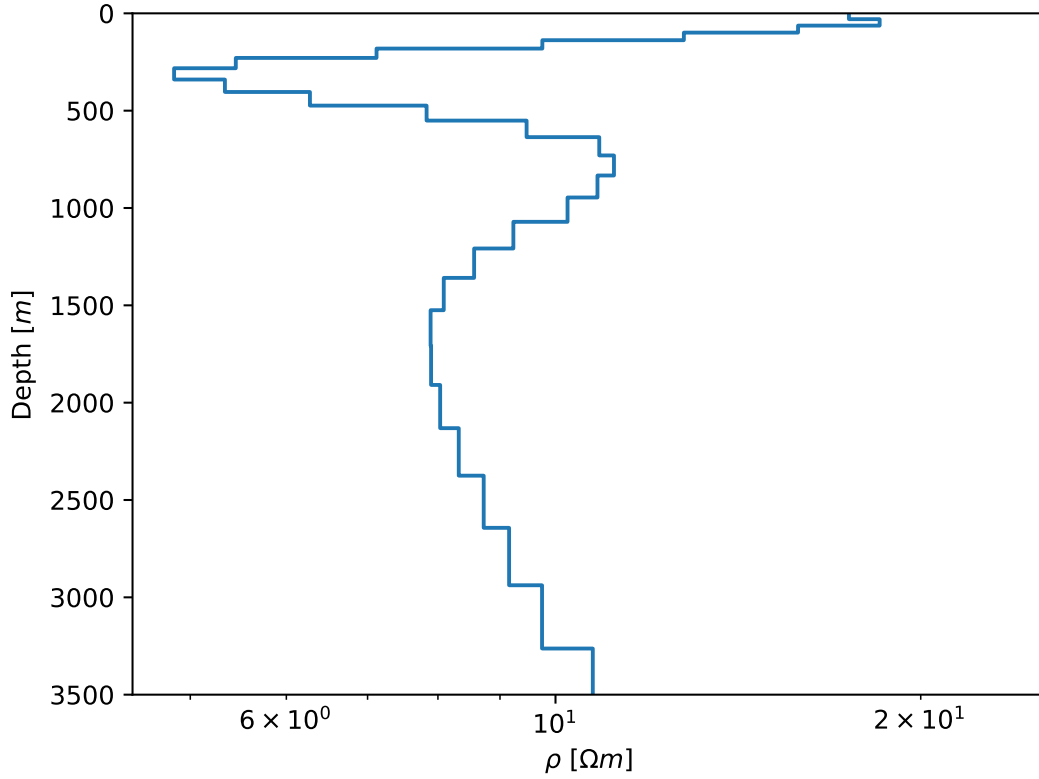
Figure 12. The layered starting model resulting from a 1D inversion of the Berdichevsky invariant of the average impedance over all sites.

some differences, but as for the comparison between the inversion with TEM estimates and without, the relative ordering remains the same. In other words, the largest distortion estimates remain large and small values remain small.

3.4 Influence of discretization

As a final test of robustness, we investigate the influence of discretization. As mentioned in the introduction, if we could model the Earth at all scales, we expect to be able to include the causative bodies for galvanic distortion. Conversely, it is possible that there are structures on the order of tens to hundred meters, that could be features in a finely discretized model, but need to be emulated through the distortion matrix in a more coarsely disretized model. To investigate this effect, we run an inversion with a model with half the horizontal and vertical discretization, i.e. $128 \times 160 \times 40$ cells, with horizontal cell lengths of 100m and a vertical discretization of 15m at the surface. All other inversion parameters are identical to the inversion run without prior information. The resulting initial and final
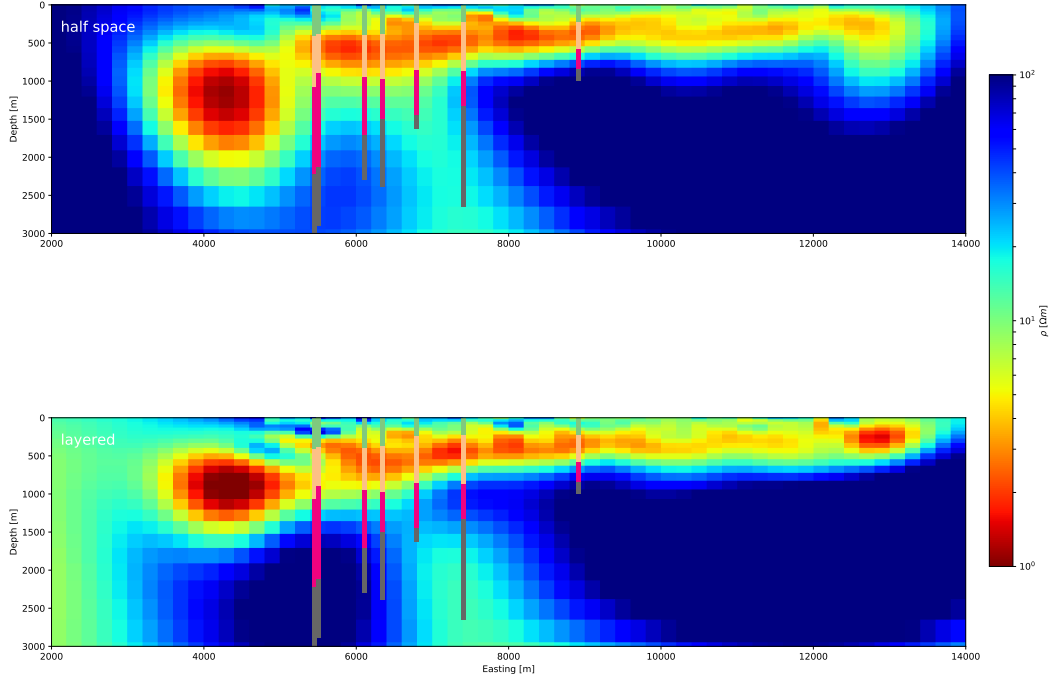
Figure 13. Comparison of the inversion result when starting from a half-space (top) and when starting from the best fitting 1D model shown in Figure 12 (bottom).

RMS, model roughness and distortion regularization values (not shown) are very similar to the results of the corresponding coarse inversion run and a comparison of the models is shown in Figure 15.

The comparison confirms the results of our previous experiments. While there are some differences in how the main conductive structures are imaged, these differences are relatively minor and within the range of what can be expected when changing the parameters for an ill-posed inverse problem. The more finely discretized model appears to reveal more fine scale internal structure of the conductive layer. However, the equivalent data misfit for the two models suggests that this is mostly a visual feature and that the data cannot resolve such fine variations. A formal resolution analysis or sensitivity study could substantiate this impression, but the inherent resolution capabilities of magnetotellurics are not the focus of this paper. For this study our conclusion is that a smaller discretization does not have a very strong impact on the model when inverting MT data with distortion correction.
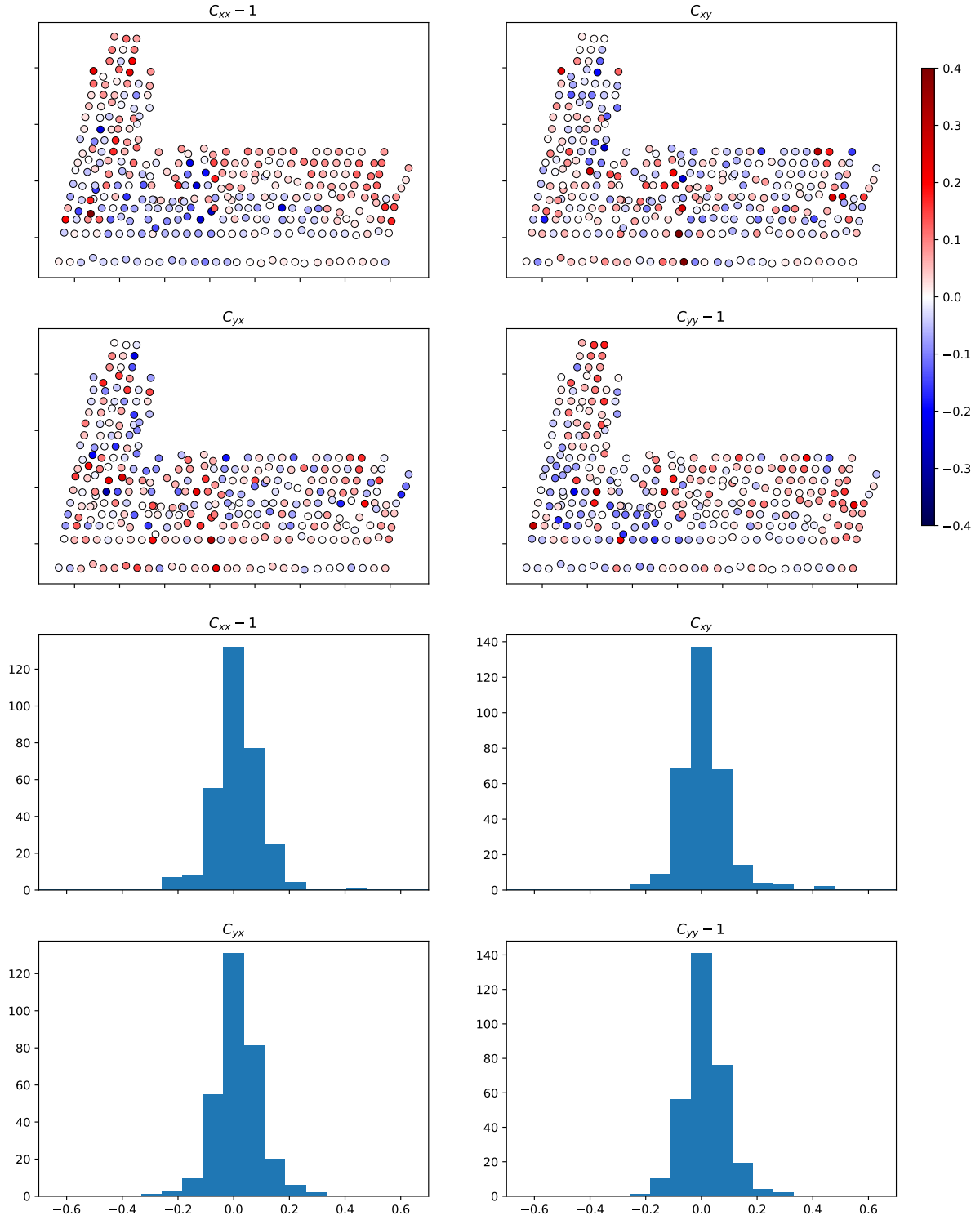
Figure 14. Convergence of the inversion runs for four different scenarios: Without using the prior distortion information from TEM and no distortion correction (blue), without prior distortion and correcting for distortion in the inversion(red), using the prior information from TEM and without distortion correction (green) and using TEM distortion and correcting for distortion (magenta).
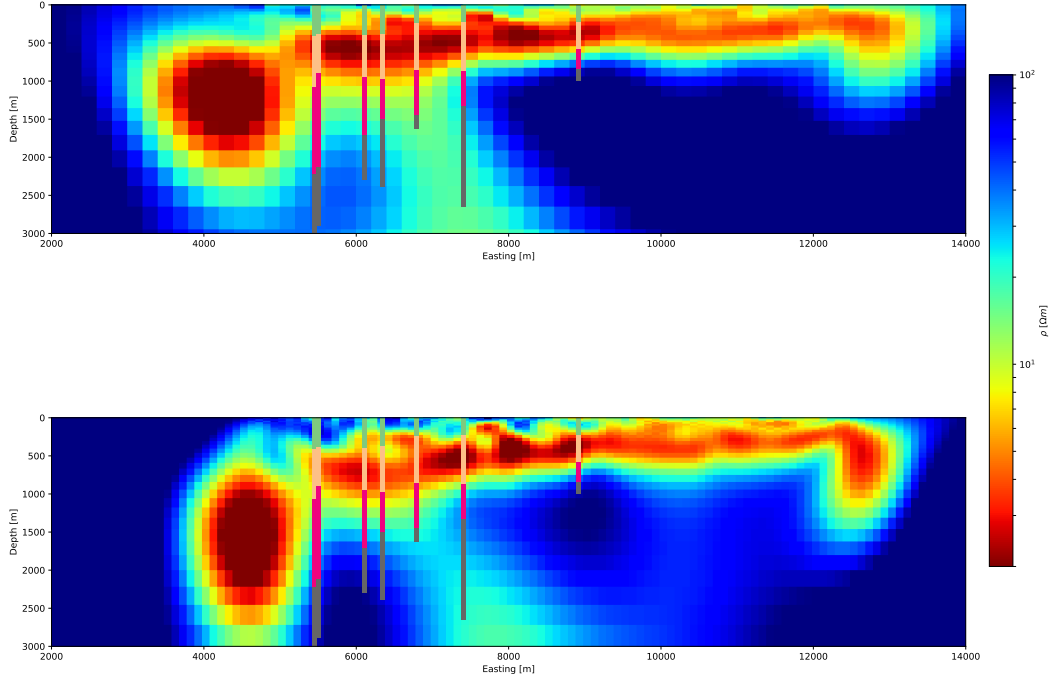
Figure 15. Comparison of the inversion result when starting from a half-space (top) and when starting from the best fitting 1D model shown in Figure 12 (bottom).

The same observation applies to the recovered distortion estimates (Figure 16). As for all previous experiments, we observe some differences in the values of the estimated distortion, but the general characteristics remain stable. Also similar to previous experiments the changes in the diagonal elements appear to be more pronounced than for the off-diagonal distortion estimates. Thus the chosen discretization does have an effect on the estimated distortion, but not to a degree that it drastically alters the resistivity model and the resulting interpretation.

4   CONCLUSIONS

In this study we have investigated the impact of the most important factors influencing the inversion with distortion correction: prior information, inversion strategy and parameter choices, starting model and model discretization. Within the range of variations investigated here, we observe that our inver-
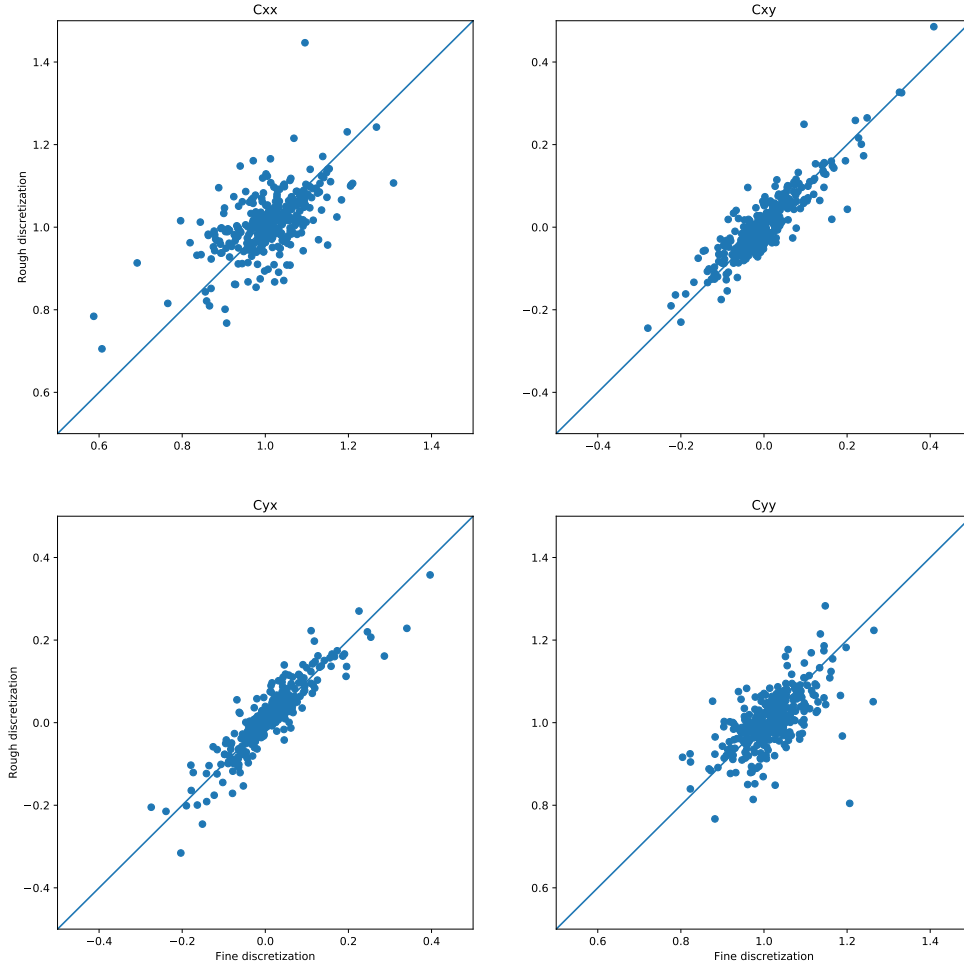
Figure 16. Comparison of the distortion estimates with a fine discretization to those retrieved with a coarse model discretization.

sion models are robust and the recovered distortion elements show some variations but retain their overall characteristics. The changes in the recovered models are comparable to those that would be expected when running a conventional MT inversion with slightly different parameters and thus suggest that the additional parameters in our scheme do not add instability to the inversion. The variations in the distortion elements illustrate that the description of the effect of small heterogeneities as a constant real valued distortion matrix is a mathematical abstraction that depends on how we choose to parametrize the Earth for the inversion. Our results also demonstrate that shifting the impedance to match the estimates of near surface resistivity from TEM measurements results in a lower initial RMS

for the inversion, but does not have a very strong impact on the final inversion results. Furthermore, all our inversion runs resulted in significant values for the off-diagonal distortion elements and a much better fit to the diagonal elements of impedance. Given the resources needed to make such additional measurements during a magnetotelluric field experiment, it might be more advantageous to use these resources for better station coverage or longer measurement times, at least for the survey under investigation here.

While we have made every effort to investigate as many influencing factors as possible and the results presented here mirror our general experience with this inversion approach, we cannot generalize these results to every conceivable situation. For example, for these inversions the site coverage was dense and regular over the area of interest. Thus all important structures were sampled by measurement at different sites. In regions with strongly heterogeneous site coverage, stronger changes to the recovered structures depending on the inversion settings are imaginable. Furthermore, the data were largely high-quality and we spend some effort culling problematic impedance estimates from the dataset before inversion. When noisy data with small error estimates are present we might see a strong influence on the distortion estimates in order to reproduce the noise. Finally, we could only test a small subset of possibilities for each influencing factors and some more extreme choices could lead to erroneous results.

However, these comments are valid for any inversion and in our experience the best remedy against spurious results is to run as many inversions with different parameter choices as feasible. Our results indicate that the additional effort needed when inverting for distortion is moderate and the improvement to the resulting models is significant. Given that it is relatively easy to add distortion correction to an existing magnetotelluric inversion, we believe that it should become a standard procedure.

ACKNOWLEDGMENTS

REFERENCES

Árnason, K., Eysteinsson, H., & Hersir, G. P., 2010. Joint 1d inversion of tem and mt data and 3d inversion of mt data in the hengill area, sw iceland, *Geothermics*, **39**(1), 13–34.

Avdeev, D. & Avdeeva, A., 2009. 3d magnetotelluric inversion using a limited-memory quasi-newton optimization, *Geophysics*, **74**(3), F45–F57.

Avdeev, D. B., Kuvshinov, A. V., Pankratov, O. V., & Newman, G. A., 2002. Three-dimensional induction logging problems, Part I: An integral equation solution and model comparisons, *Geophysics*, **67**, 413–426.

Avdeeva, A. & Avdeev, D., 2006. A limited-memory quasi-newton inversion for 1d magnetotellurics, *Geophysics*, **71**(5), G191–G196.

Avdeeva, A., Moorkamp, M., Avdeev, D., Jegen, M., & Miensopust, M., 2015. Three-dimensional inversion of magnetotelluric impedance tensor data and full distortion matrix, *Geophysical Journal International*, **202**(1), 464–481.

Berdichevskiy, M. N. & Dmitriev, V. I., 1976. Basic principles of interpretation of magnetotelluric sounding curves, in *Geoelectric and geothermal studies*, pp. 165–221, ed. Adam, A., Budapest, Akademai Kiado.

Bibby, H. M., Caldwell, T. G., & Brown, C., 2005. Determinable and non-determinable parameters of galvanic distortion in magnetotellurics, *Geophysical Journal International*, **163**, 915–930.

Caldwell, T. G., Bibby, H. M., & Brown, C., 2004. The magnetotelluric phase tensor, *Geophysical Journal International*, **158**, 457–469.

Chave, A. & Jones, A., 2012. *The magnetotelluric method*, Cambridge University press, Cambridge, UK.

Chave, A. D. & Thomson, D. J., 2004. Bounded influence magnetotelluric response function estimation, *Geophysical Journal International*, **157**, 988–1006.

Çiftçi, N. & Bozkurt, E., 2009. Evolution of the miocene sedimentary fill of the Gediz Graben, SW Turkey, *Sedimentary Geology*, **216**(3-4), 49–79.

Çiftçi, N. & Bozkurt, E., 2010. Structural evolution of the Gediz Graben, SW Turkey: temporal and spatial variation of the graben basin, *Basin Research*, **22**(6), 846–873.

Erdoğan, E. & Candansayar, M. E., 2017. The conductivity structure of the Gediz Graben geothermal area extracted from 2D and 3D magnetotelluric inversion: Synthetic and field data applications, *Geothermics*, **65**, 170–179.

Grayver, A. V., 2015. Parallel three-dimensional magnetotelluric inversion using adaptive finite-element method. part i: theory and synthetic study, *Geophysical Journal International*, **202**(1), 584–603.

Gribenko, A. & Zhdanov, M., 2017. 3-D inversion of the MT earthscope data, collected over the east central United States, *Geophysical Research Letters*, **44**(23).

Groom, R. W. & Bahr, K., 1992. Corrections for near surface effects: Decomposition of the magnetotelluric impedance tensor and scaling corrections for regional resistivities: A tutorial, *Surveys in Geophysics*, **13**(4-5), 341–379.

Hacıoğlu, Ö., Başokur, A. T., Diner, Ç., Meqbel, N., Arslan, H. İ., & Oğuz, K., in press. The effect of active extensional tectonics on the structural controls and heat transport mechanism in the Menderes massif geothermal province: Inferred from three-dimensional electrical resistivity structure of the kurşunlu geothermal field (Gediz Graben, western Anatolia), *Geothermics*.

Hübert, J., Juanatey, M. d. l. Á. G., Malehmir, A., Tryggvason, A., & Pedersen, L. B., 2012. The upper crustal

3-d resistivity structure of the kristineberg area, skellefte district, northern sweden revealed by magnetotelluric data, *Geophysical Journal International*, **192**(2), 500–513.

Jiracek, G. R., 1990. Near-surface and topographic distortions in electromagnetic induction, *Surveys in Geophysics*, **11**, 163–203.

Jones, A. G., 2011. Three-dimensional galvanic distortion of three-dimensional regional conductivity structures:Comment on "Three-dimensional joint inversion for magnetotelluric resistivity and static shift distributions in complex media" by Yutaka Sasaki and Max A. Meju, *Journal of Geophysical Research*, **116**, B12104.

Kelbert, A., Egbert, G., et al., 2012. Crust and upper mantle electrical conductivity beneath the yellowstone hotspot track, *Geology*, **40**(5), 447–450.

Meqbel, N. M., Egbert, G. D., Wannamaker, P. E., Kelbert, A., & Schultz, A., 2014. Deep electrical resistivity structure of the northwestern us derived from 3-d inversion of usarray magnetotelluric data, *Earth and Planetary Science Letters*, **402**, 290–304.

Miensopust, M. P., 2017. Application of 3-d electromagnetic inversion in practice: Challenges, pitfalls and solution approaches, *Surveys in Geophysics*, **38**(5), 869–933.

Miensopust, M. P., Queralt, P., Jones, A. G., et al., 2013. Magnetotelluric 3-d inversiona review of two successful workshops on forward and inversion code testing and comparison, *Geophysical Journal International*, **193**(3), 1216–1238.

Moorkamp, M., Fishwick, S., Walker, R. J., & Jones, A. G., 2019. Geophysical evidence for crustal and mantle weak zones controlling intra-plate seismicity–the 2017 botswana earthquake sequence, *Earth and Planetary Science Letters*, **506**, 175–183.

Newman, G. A., Recher, S., Tezkan, B., & Neubauer, F. M., 2003. 3D inversion of a scalar radio magnetotelluric field data set, *Geophysics*, **68**, 791–802.

Nocedal, J. und Wright, S., 2006. *Numerical Optimization*, Springer.

Patro, P. K., Uyeshima, M., & Siripunvaraporn, W., 2012. Three-dimensional inversion of magnetotelluric phase tensor data, *Geophysical Journal International*, p. ggs014.

Pellerin, L. & Hohmann, G. W., 1990. Transient electromagnetic inversion: A remedy for magnetotelluric static shifts, *geophysics*, **55**(9), 1242–1250.

Seyitoğlu, G. & Veysel, I., 2015. Late cenozoic extensional tectonics in western Anatolia: exhumation of the Menderes core complex and formation of related basins, *Maden Tetkik ve Arama Dergisi*, (151), 47–106.

Siripunvaraporn, W., 2012. Three-dimensional magnetotelluric inversion: An introductory guide for developers and users, *Surveys in Geophysics*, **33**, 5–27.

Soyer, W., Mackie, R., & Miorelli, F., 2018. Optimizing the estimation of distortion parameters in magnetotelluric 3d inversion, in *80th EAGE Conference and Exhibition 2018*.

Sternberg, B. K., Washburne, J. C., & Pellerin, L., 1988. Correction for the static shift in magnetotellurics using transient electromagnetic soundings, *Geophysics*, **53**(11), 1459–1468.

Tarantola, A., 2004. *Inverse Problem Theory*, SIAM, 1st edn.

Ulugergerli, E., Seyitoğlu, G., Başokur, A., Kaya, C., Dikmen, U., & Candansayar, M., 2007. The geoelectrical structure of northwestern Anatolia, Turkey, *Pure and Applied Geophysics*, **164**(5), 999–1026.

Wannamaker, P. E., 2016. Structurally controlled geothermal systems in the central cascades arc-backarc regime, Oregon, Tech. rep., Univ. of Utah, Salt Lake City, UT (United States). Energy and Geoscience .